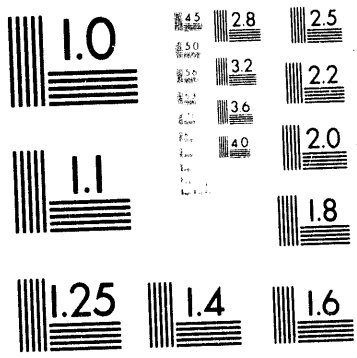
1.0
1.1
1.25
1.4
1.6
1.8
2.0
2.2
2.5
2.8
3.2
3.6
4.0
4.5
5.0

1 of 1

UNIVERSITY OF WISCONSIN

CENTER FOR PLASMA THEORY AND COMPUTATION

REPORT

Transport Properties of Interacting Magnetic Islands in Tokamak Plasmas

T.A. Gianakon, J.D. Callen and C.C. Hegna

Nuclear Engineering & Engineering Physics
and Physics Departments
University of Wisconsin-Madison
Madison, Wisconsin 53706

October 1993

UW-CPTC 93-7

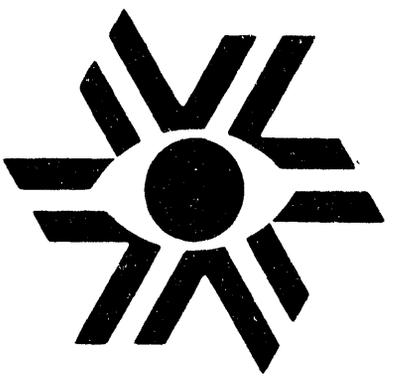

MADISON, WISCONSIN 53706-1687

Transport Properties of the Interacting Magnetic-Island Model of Tokamak Plasmas

T. A. Gianakon, J.D. Callen, C.C. Hegna
University of Wisconsin-Madison
1500 Johnson Drive, Madison, WI 53706-1687

This paper explores the equilibrium and transient transport properties of a mixed magnetic topology model for tokamak equilibria. The magnetic topology is composed of a discrete set of mostly non-overlapping magnetic islands centered on the low-order rational surfaces. Transport across the island regions is fast due to parallel transport along the stochastic magnetic field lines about the separatrix of each island. Transport between island regions is assumed to be slow due to a low residual cross-field transport. In equilibrium, such a model leads to: a nonlinear dependence of the heat flux on the pressure gradient; a power balance diffusion coefficient which increases from core to edge; and profile resiliency. Transiently, such a model also exhibits a heat pulse diffusion coefficient larger than the power balance diffusion coefficient.

Pacs numbers: 52.25.Fi, 52.55.Fa, 52.30.Jb,52.65.tz.

I. Introduction

The development of realistic models for plasma transport processes remains a key issue for characterizing toroidal confinement systems. However, many of the transport models in tokamak plasmas rely on the existence of a well defined toroidally symmetric magnetostatic equilibrium.[1] The introduction of magnetic islands caused by symmetry-breaking magnetic perturbations would alter much of the macroscopic phenomenology of tokamaks. Moreover, most stability, turbulence and turbulent transport studies do not account for the effects of an altered magnetic topology.

A new paradigm for the "equilibrium" of tokamak plasmas has been put forth,[2,3] wherein a set of interacting magnetic islands is used to describe the general state of the magnetic topology. The model is an attempt to describe an intermediate state of magnetic topology where a time-varying mix of topologically closed toroidal flux surfaces, magnetic islands, and regions of magnetic stochasticity are present. This is to be contrasted with the more standard presumption of magnetic fluctuation induced transport, where globally stochastic magnetic fields produce the dominant plasma transport processes.[4,5]

The underlying formulation for this model is based on a neoclassical modification to the magnetohydrodynamic (MHD) equations.[6] Viscous forces in toroidal plasmas cause the addition of a parallel electron viscous stress force in the projection of Ohm's law along the magnetic field. The parallel viscous force produces an equilibrium parallel plasma current proportional to the cross-field pressure gradient, the bootstrap current. This addition to the Ohm's Law provides access to pressure gradient free energy for the resistive reconnection of magnetic field lines,[6,7] and the appearance of magnetic islands.[2,6,8] Additionally, a stochastic layer, due to the presence of distinct islands across the plasma extent with different helicities, is generated about the separatrix of each island.[9] Rapid parallel transport then flattens the density and temperature profiles across each stochastic layer, and, in the absence of a heat source within the island separtrix, across each island. The flattenings of these profiles then modify the bootstrap current and ultimately affect each island's width. Model equations describing the growth and interaction of these bootstrap current driven magnetic islands have been derived[2,3] and are summarized in the next section (see ref. 2 for a detailed discussion of their theoretical basis.)

Since the description of such an "equilibrium" configuration populated with many magnetic islands is so complex, it is very difficult to accurately predict global transport properties using analytical methods. However, numerical simulations of the model equations can be used to uncover some salient features of this mixed topology model. In the numerical simulations, a set of magnetic evolution equations is used to describe the time-variation of the spatial extent of a finite set of magnetic islands and stochastic layers across the plasma extent. In the differing topological regions, a model transport equation for the plasma pressure is used to describe the pressure evolution. Details pertaining to the numerical implementation of this model are discussed in Section III.

In Section IV, the results of numerical simulations of this interacting island model are presented which explore both the steady-state and transient properties of the model. In the final section, the basic properties are reduced to a few key observations which should be applicable generally to mixed topology models.

II. Model Equations

In purely resistive MHD models, magnetic islands can appear through tearing instabilities caused by large equilibrium current gradients located near rational magnetic surfaces.[10] In present day tokamaks, such modes are generally found to be stable, i.e., $\Delta' < 0$, where Δ' is the tearing mode matching parameter. However, in long collision mean free path (banana regime) plasmas, parallel viscous stresses (between trapped and untrapped particles) and parallel viscous forces (which cause poloidal flow damping and the bootstrap current) become important and a neoclassical MHD formulation is relevant.[6] Stability studies based on neo-classical MHD indicate that when the product of the radial pressure gradient and the radial shear in the q-profile $(dp/dr)(dq/dr) < 0$ (which is generally true for tokamaks), the radial pressure gradient will cause magnetic tearing through self-consistent fluctuations in the bootstrap current.[6,7] When the amplitude of the mode increases such that the resulting magnetic island has a width in excess of the linear tearing layer, the mode evolves in a quasilinear regime.[11,12]

Model equations for a set of interacting magnetic islands in the quasi-linear regime for an axisymmetric tokamak have been developed following

a standard Rutherford-like tearing-mode methodology.[2,3] The modification due to neoclassical effects introduces a bootstrap current drive mechanism for the destabilization of each island. The resulting equation for each magnetic island is given by[2,3]

$$\frac{\mu_0}{\eta_{nc}} \frac{1}{g^{\Phi\Phi}} \frac{dw_i}{dt} = 0.6\Delta_i' + \frac{w_c}{(w_i^2 + |\delta\tilde{w}_i|)^{0.5}} \tag{1}$$

where the subscript i refers to the island resonant at the $q = m_i/n_i$ rational surface, η_{nc} is the neoclassical resistivity, $g^{\Phi\Phi} = |\nabla\Phi|^2$ is a metric element evaluated at the rational surface in the unperturbed geometry, w_i is the island half-width in flux coordinates, Δ_i' is the tearing mode matching condition, $|\delta\tilde{w}_i|$ is the stochastic layer extent from the island separatrix [see Eq. (3) below], and w_c is a parameter of the form

$$w_c = 1.4\sqrt{\epsilon}\beta_\theta L_p^{-1}/L_q^{-1} \tag{2}$$

where $\epsilon = r/R$ is the aspect ratio, $\beta_\theta = 2\mu_0 p/B_\theta^2$ is the poloidal beta, and $|\nabla\Phi|^{-1}L_q = dq/d\Phi$ and $L_p^{-1} = |\nabla\Phi|^{-1}dp/d\Phi$ are the inverse scale lengths of the q-profile and the pressure profile evaluated on the topologically toroidal magnetic flux surfaces located outside but near the island separatrix. Numerically, the pressure gradient will be based on the pressure difference between the two immediately adjacent islands.

Equation (1) represents an average of Ohm's law over the region through and outside a magnetic island.[2,3] The term on the left is caused by the inductively driven electric field contribution to Ohm's law due to the growing magnetic island. The first term on the right comprises the stabilizing effect of magnetic field line bending, which for this particular model is taken as $\Delta_i' = -2m_i/r_s$, where m_i (assumed > 1) is the poloidal mode number of island i and r_s is the radial location of the rational surface in the unperturbed geometry associated with island i. The final term represents a perturbation of the bootstrap current due to the presence of the island but with a modification from the flattening of the pressure profile via a stochastic layer (the $\delta\bar{L}_i$ term) about the separatrix of the island. The island equation is derived under the assumption that the island evolution timescale is slow compared to the pressure diffusion time scale. Specifically, the pressure profile near the island is constructed by assuming rapid transport along field lines (so that a flat pressure profile exists in the stochastic layer). Furthermore, the absence of heat sources or sinks within the separatrix of the island implies a flat pressure profile across the island.[13]

Physically, a stochastic layer is generated because an island with incom-

incommensurate helicity breaks the two-dimensional symmetry of the primary island. An estimate for the value of $\delta\bar{\psi}_i$, the extent of the stochasticity in terms of the poloidal flux, based on the width of secondary islands resonant at the separatrix of the primary magnetic island has been used.[9] The width of this stochastic layer about the separatrix of island i at $q_i = m_i/n_i$ caused by a magnetic island of half-width w_j $(j \neq i)$ at the resonant surface $q_j = m_j/n_j$ is given by

$$\delta\bar{\psi}_i = \frac{w_j^2}{\Gamma(2M)} \frac{exp(-\pi/2\Delta)}{(\Delta/2)^{2M+1}}, \tag{3}$$

where $M = m_j/m_i$, $\Delta = |n_i w_i/\Delta_{ij} n_j|$, and Δ_{ij} is the distance (in terms of the poloidal flux) between the two rational surfaces associated with island i and island j. In fact, Eq. (1) implies the generation of a stochastic layer about the primary island due to all other magnetic islands. However, the effect of more than one incommensurate helicity on the width of the stochastic layer is not easily determined analytically. Therefore, for the purposes of this analysis, the stochastic layer for each island will be calculated based on the incommensurate magnetic perturbation that generates the largest such layer, i.e.,

$$|\delta\bar{\psi}_i| = \max\left[\delta\bar{\psi}_j\right] \text{ for } j = 1, N : i \neq j. \tag{4}$$

where N is the total number of islands.

The original model by Hegna and Callen[13] has been extended to account for the reduction in the bootstrap current between a pair of islands due to the shrinkage in the fraction of non-stochastic surfaces between the islands.[3] The model equation for each island is of the form

$$\frac{\mu_0}{\eta_{nc}}\frac{1}{g^{\Phi\Phi}}\frac{dw_i}{dt} = 0.6\Delta_i' + w_e\left[\frac{(d_{i-1,i}+d_{i,i+1})}{w_{eff,i}} - \frac{d_{i-1,i}}{\Delta_{i-1,i}-w_{eff,i-1}} - \frac{d_{i,i+1}}{\Delta_{i,i+1}-w_{eff,i+1}}\right], \quad (5)$$

where the subscript i indicates the primary island and the subscripts $i-1$ and $i+1$ indicate the immediately adjacent islands. Physically, the first term proportional to w_e represents the previously outlined bootstrap current drive mechanism. The two additional terms proportional to w_e represent a reduction in the drive mechanism on the two sides of the island since adjacent islands that are distance $\Delta_{i-1,i}$ and $\Delta_{i,i+1}$ away reduce the radial range over which the primary island helically distorts the magnetic structure around it.

Additionally, an effective island width is introduced as

$$w_{eff,i} = (w_i^2 + |\delta\bar{\psi}_i|)^{0.5}, \quad (6)$$

where w_i is the island half width and $|\delta\bar{\psi}_i|$ is the largest stochastic layer about island i. The coefficients $d_{i-1,i}$ and $d_{i,i+1}$ are introduced to suppress

half the bootstrap current drive when two adjacent islands overlap and are given by

$$d_{i,j} = \begin{cases} 0.5, & w_{eff,i} + w_{eff,j} \leq \Delta_{ij} \\ 0.0, & \text{otherwise} \end{cases} \tag{7}$$

where Δ_{ij} is the distance between islands i and j.

This modification to the original island evolution equation is motivated by the fact that as two adjacent islands approach an overlap condition, very few of the magnetic surfaces remain non-stochastic. Since the pressure gradients (and the resulting bootstrap current) are sustained only on the non-stochastic surfaces, the reduction of the bootstrap current drive must accompany the disappearance of these non-stochastic surfaces.

In the original formulation of this problem, the pressure transport was assumed to be infinitely fast compared to the magnetic island evolution time scale. As such, a gross simplification to the pressure dynamics was made. In the non-stochastic region beyond both the island and the stochastic layer about the island, the pressure gradient was fixed as a consequence of a constant heat flux boundary condition (assuming no pressure sources or sinks exist in the vicinity of the island).[13] When two islands overlapped, the rapid transport along field-lines then caused an immediate flattening of the pres-

sure profile. While such a procedure poses no inherent difficulties for only two interacting islands, such a model is insufficient for multiple islands where the equilibration of pressure across two overlapping islands may have a profound effect on the gradients about neighboring islands. To portray this pressure dynamic more realistically, the original model is expanded to include a pressure evolution equation in cylindrical geometry. Namely, a diffusion equation of the form

$$\frac{\partial p}{\partial t} = \frac{1}{r}\frac{\partial}{\partial r}\,\backslash(r)\,r\frac{\partial p}{\partial r} + sources \tag{8}$$

where $\backslash$ is the pressure diffusion coefficient and is taken to be a function of the topological character of the region. Specifically, the diffusion coefficient is taken to be 10^4 m^2s^{-1} in regions dominated by stochastic surfaces and 1 m^2s^{-1} in regions described by non-stochastic surfaces. The source term of Eq. (8) is normally set to zero except to implement a constant heat flux at the inner boundary condition and to simulate off axis heating experiments. The pressure is fixed at the outer boundary which is the plasma edge. While such a cylindrical approximation is a gross over-simplification of the actual pressure dynamics in the full toroidal geometry, it nonetheless provides in-

teresting insights into the macroscopic transport properties of this model.

III. Numerical Implementation

To explore the macroscopic features of this model, a cylindrical annulus of plasma is assumed with a specified heat flux at the inner radius and a fixed pressure at the edge. The numerical values of the inner and outer radii are determined from the equilibrium q-profile and based on the rational surfaces defined by q=1.099 and q=3.501. The choice of these two rational surfaces is arbitrary, but avoids the heating profile and sawteeth associated with the plasma core and peculiarities associated with the plasma edge—features that are not presently included in the model. No distinction will be made between density and temperature; instead the pressure will be evolved via Eq.(8) with the two disparate values of χ for stochastic and non-stochastic regions. Further details of the numerical implementation of the pressure evolution equation are discussed below.

The equilibrium q-profile is not evolved, but is assumed to be

$$q = \left(1 + (r/a)^2\right)^2 \tag{9}$$

where r is the plasma radius, and a is the plasma minor radius. While the

above assumption does not provide for a possible change in the equilibrium q-profile due to the presence of islands, this simplifying approximation has the advantage of allowing for the ready mapping between the flux coordinates associated with the model equation and the cylindrical coordinates of the pressure evolution model. Specifically, the equilibrium flux is related to the q-profile (in a large aspect ratio expansion) by

$$\Phi = \frac{1}{2}\left[1 - q^{-1/2}\right] \tag{10}$$

where the flux variables and island widths have been normalized by the factor $B_{\phi 0}a^2$, the product of the equilibrium toroidal magnetic field on axis and the square of the minor radius. Specifically, we have assumed $B_{\phi 0} = 5$ T and $a = 0.8$ m (Tokamak Fusion Test Reactor[14]-like parameters) throughout this analysis. The radial extent of a specified island is determined by combining Eqs. (9) and (10) and is given by

$$r = \left[-1 + \frac{1}{1 - 2\mathcal{O}}\right]^{1/2} \tag{11}$$

where $\mathcal{O}$ is given by

$$\mathcal{O} = \Phi_0 \pm \left[w_{eff}^2 + w^2\frac{(1 + \cos(m\theta))}{2}\right]^{1/2} \tag{12}$$

in which Φ_0 is the equilibrium flux at the particular rational surface, w_{eff}

is the effective island width which includes the stochastic layer, w is the island width in the absence of a stochastic layer, m is the poloidal mode number of the island, and θ is a poloidal angle. Figure 1 is a projection of the plasma cross-section at a fixed toroidal angle and illustrates a typical set of islands based on 10 MW of centrally injected power. The uniformity of phase between the island structures should not be construed as reality; it stems from the lack of phase information in the original model.

One shortcoming of the neoclassical MHD model is that it predicts that a magnetic island of finite width will form at every rational surface. A configuration with a dense set of islands necessarily implies inevitable island overlap, complete stochastization of the magnetic field lines, and a flat pressure profile due to rapid parallel transport along the field lines. Furthermore, this violates the isolated island assumption used to derive the island evolution equation. However, kinetic effects (which are outside the present formulation of the model) would likely suppress high m magnetic islands. To model this effect, the number of islands is limited to those with widths approximately larger than an ion banana width ($\sim 0.01\,a$), which will amount to choosing islands with a toroidal mode number n less than 6.

Additionally, a resistive time step, defined as

$$\tau_r = \frac{\mu_0 a^2}{1.2\eta_{nc}}, \tag{13}$$

is introduced and given a fixed value for each simulation. Values of τ_r = 1, 10, or 100 s have been used. The spatial variation of η_{nc} with the plasma temperature ($\propto T^{-3/2}$) has been ignored. The additional complication of a radially varying resistivity only modifies the time scale of the dynamical growth and decay of each island, but does not affect the "saturation" width of the islands. As a consequence, the choice of τ_r will have a bearing only on transient features of the model.

Up to now, the pressure evolution equation has simply been specified according to Eq. (8) with a brief parenthetical comment on stochastic regions being modelled by a large value of χ, the pressure diffusion coefficient. For the purposes of this analysis, the largest annular extent of an island, which is time varying, is defined as the combination of the island width and the stochastic layer width and is given by Eq. (6). This annular extent of the island is characterized by the diffusion coefficient of a stochastic region. This does not imply that the field is completely stochastized throughout the island, but rather that the stochastic layer about the island provides a rapid

mechanism for the heat transport around the island. Such an approximation ignores both the heat transport out of the island proper as well as the poloidal structure of the island. Neither approximation is particularly compromising given a sufficiently narrow island and the effective smoothing of the poloidal structure due to the stochastic layer.

The time variation of the annular extent of the island coupled to the possibility of island overlap introduces a significant complication to the numerical solution of the pressure evolution equation. To deal with this complication, two sets of grids are introduced. The first grid describes the bounding radius of each of the island annului and provides an assignment of a numerical value of χ to stochastic and non-stochastic regions, $10^{4}\,\mathrm{m^2 s^{-1}}$ and $1\,\mathrm{m^2 s^{-1}}$, respectively. Islands which overlap introduce a non-sequential ordering to this grid, which is remedied by re-ordering this grid and assigning χ in any overlap region to the χ of the stochastic region.

The second grid represents the grid on which the spatial finite differencing of the pressure evolution equation occurs and is simply a refinement of the re-ordered first grid. An equal number of points are introduced within each domain defined by the first grid. A standard finite difference equation is then

evaluated for each radial point and a fully implicit scheme is introduced for the time variation. At each new time step, because of the time variation of the radial extent of each island, a complete re-evaluation of the entire set of coefficients which define the finite difference equations is required. However, the pressure at each grid point does not change, though the location of the point may have changed. Such a procedure is justified, if a time step is chosen such that the radial variation in each grid point introduces only a small amount of transport relative to the transport associated with the pressure evolution equation. For the following analysis, the timestep has been fixed to $1.0 \times 10^{-5}\,\tau_r$.

At each time step, the evolved pressure profile modifies the model equation for each island by introducing changes in w_c via β_{pi} and L_p. In a rudimentary attempt to remain consistent with the ordering of the model equations, β_{pi} is evaluated based on the pressure at the island center and L_p is based on the pressure difference between the centers of the two immediately adjacent islands. The model equations are stepped forward with the package LSODE.[15]

IV. Results

For the interacting island model based on Eqs. (2 – 8), numerical simulations have been conducted which attempt to emulate two classes of experiments. First, basic incremental power scans for both core and off-axis heating have been completed to provide an overview of the steady-state features of this model. These features include determination of: the islands responsible for stochastic layer generation; pressure profiles for core and off-axis heating; radial dependence of fluctuation levels; and effective power balance thermal diffusion coefficients (χ_{PB}). The second series of simulations model transient experiments which measure heat pulse propagation. Specifically, χ_{HP}, the transient heat pulse diffusion coefficient, has been computed for this particular model.

Figure 1 illustrates a typical set of islands for 10 MW of injected power in the core region. Each island's width scales roughly with $1/m$, the poloidal mode number of the island. Also, the dominant island which generates the largest stochastic layer about each island is not restricted to the nearest neighbor but rather depends strongly on the distance to each of the surrounding islands and their widths. Except for variations in the island widths

and changes in the specific island which generates each of the stochastic layers, similar structures have been observed over the range of power from 1 MW to 1000 MW.

Before the equilibrium features of this model are detailed, a brief description of the evolution of the pressure profile to the "equilibrium" state is warranted. At the start of a simulation, the islands are initialized to a small, but finite width and the pressure profile is initialized to an analytical profile based on the injected power and a constant diffusion coefficient across the plasma. Figure 2 illustrates the pressure profile at three times during the evolution of the profile for 40 MW of injected power and $\tau_r = 1$ s. The flat spot in each profile corresponds to the location of one or more islands and is based on the combination of the island width at the O-point and the stochastic layer width. In reality, the profile would not exhibit the sharply varying "stair-step" character of Fig. 2, but instead would vary smoothly as χ varied smoothly through the stochastic region. In this particular case, the island widths and the pressure profile evolve on a sufficiently similar time scale ($\chi \tau_r / a^2 \sim 1.5$), so that the pressure profile uniformly approaches the equilibrium profile from below. However, as depicted in Fig. 3, an increase

in τ_r dramatically changes the rate of evolution of the pressure, but not the equilibrium pressure. Namely, the slow growth of the island widths at large τ_r leads to a large fraction of non-stochastic surfaces early in the simulation. The non-stochastic surfaces act as the primary transport barrier and cause a larger peak pressure. Eventually, as the islands reach their saturated widths, the pressure profile relaxes to the equilibrium profile and becomes independent of τ_r.

Figure 4 illustrates typical "equilibrium" pressure profiles for four cases: a) 20 MW of power injected in the core; b) 40 MW of power injected in the core; c) 20 MW of power injected in the core and 20 MW of power injected at the half-radius; and d) 20 MW of power injected in the core and 80 MW of power injected at the half-radius. In cases c) and d), which represent off-axis heating, the system is allowed to equilibrate at the power level associated with the core prior to the addition of power at the half radius. Outside the half radius, the pressure profile for case a) and case c) match exactly due to the same quantity of heat passing through the region. Similarly, inside the half-radius, the pressure profile for case a) and case c) match, except for a constant offset due to the heating at the half-radius. Case d) represents the

equilibrium profile for a case where the dominant heating is off-axis. Even with the dominant heating off-axis, the pressure profiles do not appear to deviate significantly from a basic profile shape, i.e., the profile is "resilient."

In order to characterize the degree to which island regions predominate in the annular region being considered, f_{ns}, the fraction of non-stochastic surfaces across the annular extent, was computed as a function of the injected power. Figure 5 illustrates the scaling of f_{ns} and p_{peak}, the peak pressure at the inner radius, as a function of P_{inj}, the injected power. Functionally, these two curves take the form $f_{ns} = (P_{inj}/0.68)^{-0.44}$ and $p_{peak} = (P_{inj}/4.1(10^{-8}))^{0.55}$, where P_{inj} is measured in units of MW. Phenomenologically, at low power levels, both the peak pressure and the associated gradients are small. Consequently, the island widths saturate at small values and the total fraction of good surfaces is large. As the power is increased incrementally, the peak pressure also increases but at a significantly reduced increment; the confinement degrades with power. If the island sizes were unaffected by the pressure gradient, then the peak pressure would have scaled linearly with the injected power. Instead, the steepening of the gradients produces larger islands and a decrease in the fraction of non-stochastic sur-

faces.

A simple interpretation of these results can be made using a recently developed model to describe transport through a mixture of topological regions.[16] In the present model the heat flux, q, is continuous across each topological region. The pressure drop across a particular region of the plasma is then given by $\Delta p_i = q\Delta r_i/\chi_i$, where χ_i is the heat transport coefficient of region i with radial extent Δr_i. The total pressure drop amounts to a summation over each of the regions, $\Delta p = \sum_i \Delta p_i = q\sum_i \Delta r_i/\chi_i$. An average transport coefficient is then defined as $\chi_{av} = q\Delta r/\Delta p$, where Δr is the total radial extent. The average transport coefficient is then $\chi_{av} = (\sum_i f_i/\chi_i)^{-1}$, where f_i is the fractional area described by χ_i. In the present model, the transport in the stochastic region is much larger (factor 10^4) than in the non-stochastic region; hence, $\chi_{av} \simeq \chi_{ns}/f_{ns}$. Since the fraction of surfaces depends on the radial extent of the islands and the islands evolve according to the pressure gradient, the average transport coefficient naturally has a nonlinear dependence on the input power and increases with increasing input power.

Figure 6 extends this notion of a nonlinear thermal diffusion coefficient

by plotting the heat flux through the center of several selected islands versus the pressure gradient across the island. The heat flux is computed based on the injected power passing through the cross-sectional area at the specified radial location, $q = P_{inj}/(2\pi)^2 R_0 r$, while the pressure gradient is based on the pressure drop across the centers of the two adjacent islands, as per the island drive mechanism. As depicted in Fig. 7, the power balance diffusion coefficient is computed as the ratio of these two quantities, $\chi_{PB} = q/(-\nabla_r p)$. Figure 8 plots χ_{PB} as a function of the radial location for various levels of injected power and Fig. 7 illustrates χ_{PB} as a function of P_{inj} at $r/a = 0.5147$. A notable trend in Fig. 6 is that the relative steepness of each curve increases with an increase in radial location, which is then manifested in Fig. 8 as a weakly increasing diffusion coefficient from the core to the edge. This feature is driven by the original choice of the q-profile which introduced a higher density of low order rational surfaces, and hence islands, with increasing radius.

The "equilibrium" properties of the global profiles have been considered, but an exploration of the fluctuation properties of the model are warranted due to early predictions[2] that the model might exhibit, what has been termed, "magnetic bubbling" in the island widths and the pressure profile. The term

magnetic bubbling is used to signify fluctuations which arise from the interaction and overlap of neighboring islands and not the rotation of the island structure past a fixed diagnostic. Typical rms pressure fluctuation levels at the center of each island are on the order of $\tilde{p}_{rms}/p \simeq 10^{-5}$ and are more representative of numerical noise as opposed to any real fluctuation. In contrast, the fluctuation level of a static island rotating past a fixed diagnostic is much larger. Such a diagnostic instead gives a fluctuation amplitude which depends on the size of the island, $\tilde{p}_{rms}/p \simeq 0.1w/L_p$.[17] Figure 9 illustrates the expected fluctuation levels from such a diagnostic based on the saturated island widths for 40 MW of injected power. Strictly speaking, each fluctuation level is valid only for a single isolated island;[17] it's not clear how to calculate the fluctuation level where the islands are hovering near overlap conditions, as is the case here.

The final set of numerical simulations which have been conducted explore the transient features of this model by introducing a heat pulse at the inner radius of the simulation volume. In each case, the injected power at the central radius is doubled for the pulse duration of 10^{-4} s. Prior to the injection of the pulse, the system of equations is stepped forward in time

until a steady-state is reached. The pulse is then introduced and the pressure difference between the steady state and the pulsed profile is recorded as a function of time for selected radii. Figure 10 illustrates the computed pressure difference for 30 MW of injected power. Each curve is characterized by a sharp rise in the pressure as the heat pulse reaches that radial location and is then followed by a long decay. At this particular power, the heat-pulse features are readily observed at all radial locations except for the outer radii where the diffusive spreading of the pulse and numerical noise mask the ever smaller heat pulse. This effect becomes more pronounced at higher power levels and precludes the calculation of any radial dependent features of the heat pulse.

As in heat pulse experiments, χ_{HP} is computed by measuring the time-to-peak delay at several radial locations, where the time-to-peak delay is the time lag between the start of the pulse and the peaking of the pressure at a particular radial location. Figure 11 illustrates the dependence of the time-to-peak delay for various levels of injected power plotted versus $(r - r_s)^2$, the square of the distance between the source location and the radial location. The initial slope of each of these curves is then related to the heat pulse

thermal diffusion coefficient by $\chi_{HP} \simeq \Delta(r - r_s)^2/3\Delta t_p$.[18,19] Figure 12 illustrates the dependence of χ_{HP} on the injected power for various levels of τ_p based on curves similar to those in Figure 11.

V. Discussion

Several basic observations can be made with this model. First, if such a model is valid then islands such as the 2/1 should be observable as flat spots in the temperature profile. For instance, at 10 MW of power the q=2/1 island plus stochastic region has a maximum extent of 8 cm and even at 1 MW the q=2/1 has an extent of 1 cm. However, these island sizes and power levels should be carefully interpreted based on the initial assumption of a 1 m^2s^{-1} diffusion coefficient across the non-stochastic regions. Increasing this diffusion coefficient by an order of magnitude would (except for the dynamics) bring the 10 MW case into the range of generating a 2 cm q=2/1 island. Some experimental observations have suggested the possibility that magnetic island-like structures may exist on low order rational surfaces in tokamak plasmas.[20-24] However, ECE (electron cyclotron emission) measurements of the electron temperature profile in TFTR do not seem to observe

such features.[25]

The second observation is that χ_{PB}, the power balance diffusion coefficient, increases with the injected power. This result is not surprising given that islands grow to larger widths with an increase in the pressure gradient and that the pressure gradients are driven by the injected power. Larger islands imply larger effective regions of stochasticity and hence smaller regions of non-stochastic surfaces. Since the non-stochastic surfaces act as the transport barrier in these simulations, a decrease in the widths of these regions necessarily leads to an increase in the average transport coefficient.

Related to this observation is the fact that χ_{PB} also weakly increases with radial location. This feature is also driven by the decreasing fraction of non-stochastic surfaces and stems from the increasing density of low order rational surfaces with increasing radius (see Fig. 1). Since the model has been limited to the formation of islands at the low order rational surfaces, predominantly fewer non-stochastic surfaces exist with increasing radius, which then results in the higher diffusion coefficient in this region.

The final observation as indicated in Fig. 12 is that χ_{HP}, the heat pulse diffusion coefficient, varies from a factor of $1.2 - 2$ times larger than χ_{PB} at

low τ_r to being the same as ∇p_B at high τ_r. A simple interpretation of this result based on a nonlinear diffusion coefficient is possible based on Fig. 7. Namely, the slope of the heat flux versus the radial pressure gradient (∇_{flux}) at any specified pressure gradient will always be larger than the associated ratio of the heat flux to the pressure gradient (∇p_B). However, ∇_{flux} is only relevant when the diffusion rate due to the growth of the islands is sufficiently similar to the diffusion rate. For instance, at low τ_r the system evolves during a transient by adjusting to the pressure gradient as per the power balance curve, which can lead to ∇_{HP} larger than ∇_{flux}. In contrast, at large τ_r the islands do not evolve during the heat pulse and consequently the heat pulse diffuses at the power balance rate. Such a nonlinear diffusion coefficient also points to what falsely might be thought to be a pressure (or heat) pinch.

In conclusion, the basic model which has been explored is that the magnetic topology is composed of two domains. The first domain is composed of a magnetic island which is surrounded by a stochastic layer about the island separatrix. The radial transport of pressure across the island is dominated by rapid transport along the stochastic magnetic field lines which flatten the pressure profile across this regime. The second domain is composed of

non-stochastic surfaces which are dominated by slow cross-field transport. A finite number of these regions are interspersed across the plasma extent based on the density of low order rational surfaces. The width of each region is determined by the pressure gradient. Specifically, the interacting bootstrap current driven magnetic island model has been used to determine the relationship between the pressure gradient and the width of the stochastic regions. However, any model that causes the region of slow transport to shrink with an increase in the pressure gradient is sufficient to produce similar results. Such a model naturally leads to a nonlinear power balance diffusion coefficient, pressure profile "resiliency," and a heat pulse diffusion coefficient which is larger than the power balance diffusion coefficient.

VI. Acknowledgments

This work supported by the U.S. Department of Energy under Grant No. DE-FG02-86ER53218.

References

[1]J.D. Callen, Phys. Fluids B **4**, 2142 (1992).

[2]C.C. Hegna and J.D. Callen, Phys. Fluids B **4**, 1855 (1992).

[3]C.C. Hegna, J.D. Callen, T.A. Gianakon, W.X. Qu, A.I. Smolyakov and J.P. Wang, Plasma Phys. Control. Fusion **35**, 987 (1993).

[4]A.B. Rechester and M.N. Rosenbluth, Phys. Rev. Lett. **40**, 38 (1978).

[5]P.H. Rebut, M. Brusati, M. Hugon and P. Lallia, in *Plasma Phys. and Controlled Nuclear Fusion Research, 1986, Kyoto* (International Atomic Energy Agency, Vienna, 1987), Vol. 2, p 187.

[6]J.D. Callen, W.X. Qu, K.D. Siebert, B.A. Carreras, K.C. Shaing and D.A. Spong, in *Plasma Physics and Controlled Nuclear Fusion Research, 1986, Kyoto*, (International Atomic Energy Agency,Vienna,1987) Vol. 2, p. 157.

[7]T.S. Hahm, Phys. Fluids 31, 3709 (1988).

[8]R. Carrera, R.D. Hazeltine and M. Kotschenreuther, Phys. Fluids **29**, 899 (1986).

[9]A.B. Rechester and T.H. Stix, Phys. Rev. Letters **36**, 587 (1976).

[10]H.P. Furth, J. Killeen and M.N. Rosenbluth, Phys. Fluids **6**, 459 (1963).

[11]P.H. Rutherford, Phys. Fluids **16**, 1903 (1973).

[12]R.B. White, D.A. Monticello, M.N. Rosenbluth, and B.V. Wadell, Phys. Fluids **20**, 800 (1977).

[13]C.C. Hegna and J.D. Callen, Phys. Fluids B **4**, 4072 (1992).

[14]R. J. Hawryluk, V. Arunasalam, M. G. Bell, M. Bitter, W. R. Blanchard, N. L. Bretz, R. Budny, C. E. Bush, J. D. Callen, S. A. Cohen, S. K. Combs, S. L. Davis, D. L. Dimock, H. F. Dylla, P. C. Efthimion, L. C. Emerson, A. C. England, H. P. Eubank, R. J. Fonck, E. Fredrickson, H. P. Furth, G. Gammel, R. J. Goldston, B. Grek, L. R. Grisham, G. Hammett, W. W. Heidbrink, H. W. Hendel, K. W. Hill, E. Hinnov, S. Hiroe, H. Hsuan, R. A. Hulse, K. P. Jaehnig, D. Jassby, F. C. Jobes, D. W. Johnson, L. C. Johnson, R. Kaita, R. Kamperschroer, S. M. Kaye, S. J. Kilpatrick, R. J. Knize, H. Kugel, P. H. LaMarche, B. LeBlanc, R. Little, C. H. Ma, D. M. Manos, D. K. Mansfield, R. T. McCann, M. P. McCarthy, D. C. McCune, K. McGuire, D. H. McNeill, D. M. Meade, S. S. Medley, D. R. Mikkelsen, S. L. Milora, W. Morris, D. Mueller, V.

Mukhovatov, E. B. Nieschmidt, J. O'Rourke, D. K. Owens, H. Park, N. Pomphrey, B. Prichard, A. T. Ramsey, M. H. Redi, A. L. Roquemore, P. H. Rutherford, N. R. Sauthoff, G. Schilling, J. Schivell, G. L. Schmidt, S. D. Scott, S. Sesnic, J. C. Sinnis, F. J. Stauffer, B. C. Stratton, G. D. Tait, G. Taylor, J. R. Timberlake, H. H. Towner, M. Ulrickson, V. Vershkov, S. Von Goeler, F. Wagner, R. Weiland, J. B. Wilgen, M. Williams, K. L. Wong, S. Yoshikawa, R. Yoshino, K. M. Young, M. C. Zarnstorff, V. S. Zaveryaev and S. J. Zweben, in Plasma Physics and Controlled Nuclear Fusion Research, Proceedings of the 11th International Conference, held in Kyoto, Japan, 1986, (International Atomic Energy Agency, Vienna, 1987), Vol. 1, p. 51.

[15]A.C. Hindmarsh, *Odepack, A Systematized Collection of ODE Solvers in Scientific Computing* , edited by R.S. Stepleman, M. Carver, R. Peskin, W.F. Ames, R Vichnevetsky, (North-Holland, Amsterdam, 1983), pp. 55-64.

[16]C.C. Hegna and J.D. Callen, Phys. Fluids B **5**, 1804 (1993).

[17]J.D. Callen, Z. Chang, R.L. Coffey T.A. Gianakon, C.C. Hegna, A.I. Smolyakov, W.X. Qu, and J.P. Wang, "Magnetic Island Effects, Inter-

actions in Tokamaks", in *Proceedings of Workshop on "Local Transport Studies in Fusion Plasmas"*, Varenna, Italy, 30 August 3 September 1993,(??????,?????,?????) "to be published."

[18]E.D. Fredrickson, J.D. Callen, K. McGuire, J.D. Bell R.J. Colchin, P.C. Efthimion, K.W. Hill, R. Izzo, D.R. Mikkelsen, D.A. Monticello, V. Pave, G. Taylor, and M. Zarnstorff., Nuclear Fusion **26**, 849 (1986).

[19]M. Solier, J.D. Callen, Nuclear Fusion **19**, 703 (1979).

[20]H. Soltwisch, W. Stodiek, J. Manickam and J. Schlüter, in *Plasma Physics and Controlled Nuclear Fusion Research, 1986, Kyoto* (International Atomic Energy Agency, Vienna, 1987), Vol. 1, p. 263.

[21]M.F.F. Nave, A.W. Edwards, K. Hirsch, M. Hugon, A. Jacchia, F. Lazzarro, H. Salzmann, and P. Smeulders, Nuclear Fusion **32**, 825 (1992).

[22]M.A. Dubois R. Sabot, B. Pégourié, H.W. Drawin and A. Geraud, Nuclear Fusion **32**, 1935 (1992).

[23]D.K. Mansfield, A.T. Ramsey, M.G. Bell, E.D. Fredrickson, F.C. Jobes, D.K. Owens, G.L. Schmidt and G. Taylor, Nuclear Fusion **33**, 1301 (1993).

[21]B. Grek, D.W. Johnson and W. Park (1993), submitted to Nuclear Fusion (1993).

[25]M.C. Zarnstorff, "Search for Radial Structures on TFTR", in *Proceedings of Workshop on "Local Transport Studies in Fusion Plasmas"*, Varenna, Italy, 30 August 3 September 1993,(?????,?????,?????) "to be published".

List of Figures

7 The power balance pressure diffusion coefficient, χ_{PB}, is defined as the ratio of the heat flux to the radial pressure gradient. In contrast, the incremental pressure diffusion coefficient χ_{flux} is defined based on the "local" slope of the curve. 45

8 The power balance pressure diffusion coefficient, χ_{PB}, weakly increases from the core to the edge region and sharply increases with the injected power. 46

9 Pressure fluctuation level based on the static rotation of an island structure past a fixed diagnostic. These fluctuation levels increase with injected power, because the island widths increase with injected power. Each fluctuation level is only strictly valid for a single isolated island, rather than the near overlapping island situation in the simulations (see Fig. 1). . . 47

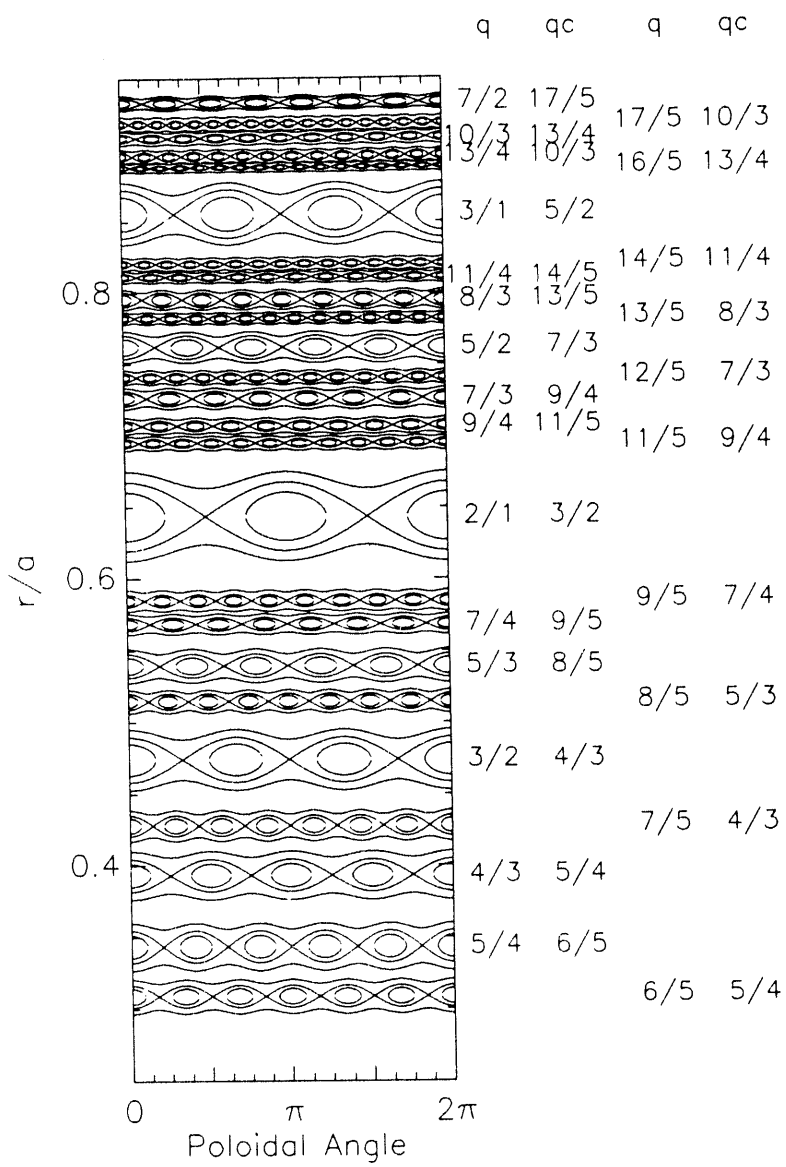

Figure 1: The poloidal island structure for 10 MW of core injected power indicates that regions of non-stochastic surfaces are dominant where the density of rational surfaces is low. The stochastic layer about each island is driven by the nearby island at q_c. The phase between islands is arbitrarily set to zero.

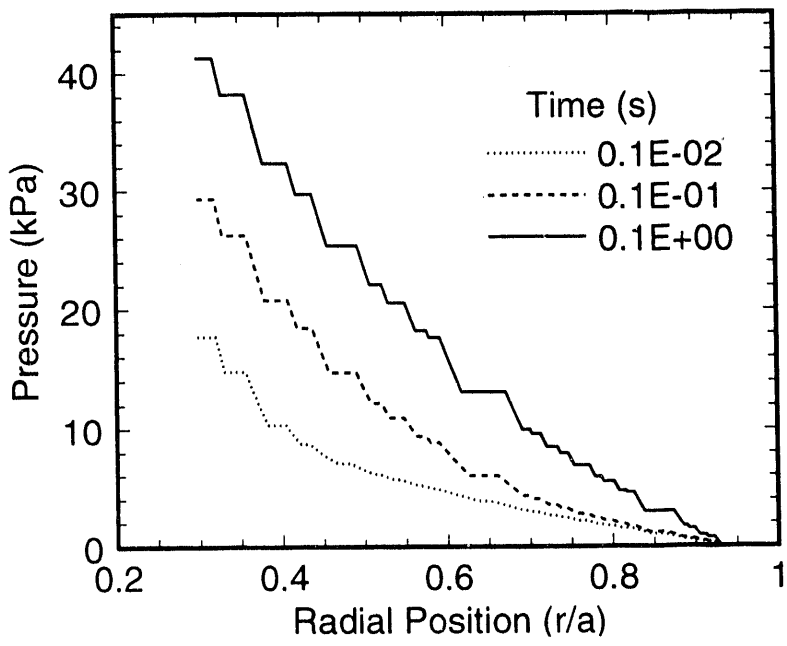

Figure 2: The pressure profile ($P_{inj} = 40$ MW) for the interacting island model exhibits flat spots across the extent of each island as the islands evolve from a small width. The flat spot comprises the maximum extent of each island as measured across the O-point and the stochastic layer.

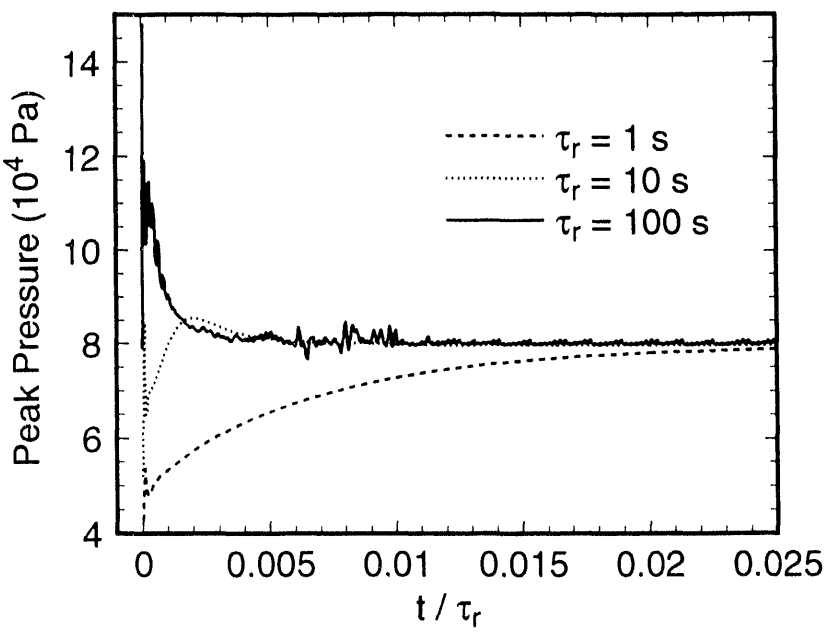

Figure 3: The evolution of the pressure profile is sensitive to the choice of τ_r, but equilibrates to the same peak pressure and hence profile. The pressure overshoot is due to the slow growth of the island widths which leads to a higher than equilibrium fraction of non-stochastic surfaces early in the simulation.

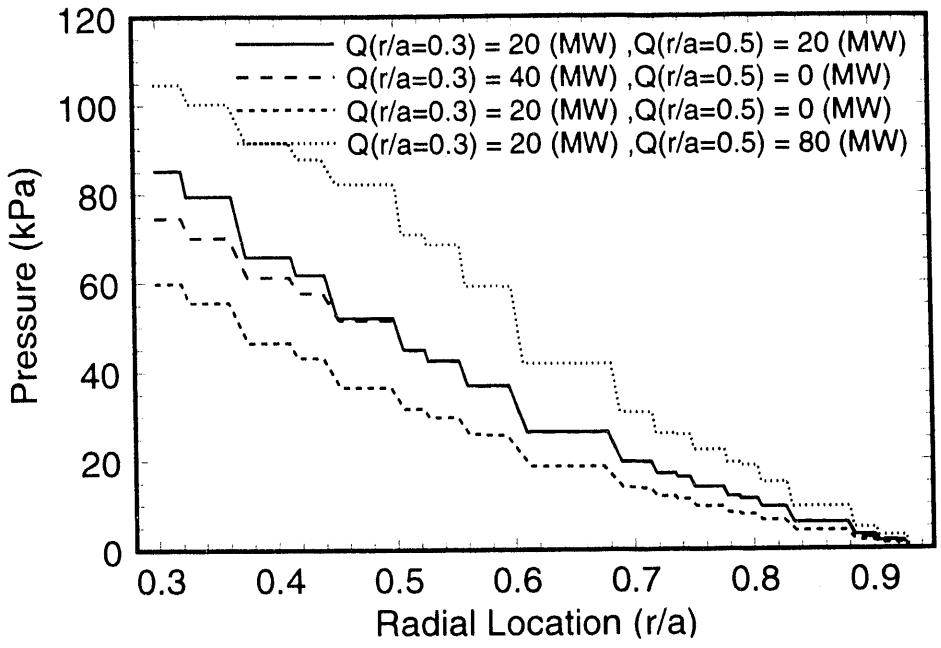

Figure 4: The pressure profile is resilient to off-axis heating. Inside the half-radius, the pressure profile for the off-axis heating case matches the 20 MW core heating case (except for a constant offset) due to the conservation of heat through the region. Likewise, outside the half-radius, the pressure profile for the off-axis heating case matches the 40 MW core heating case.

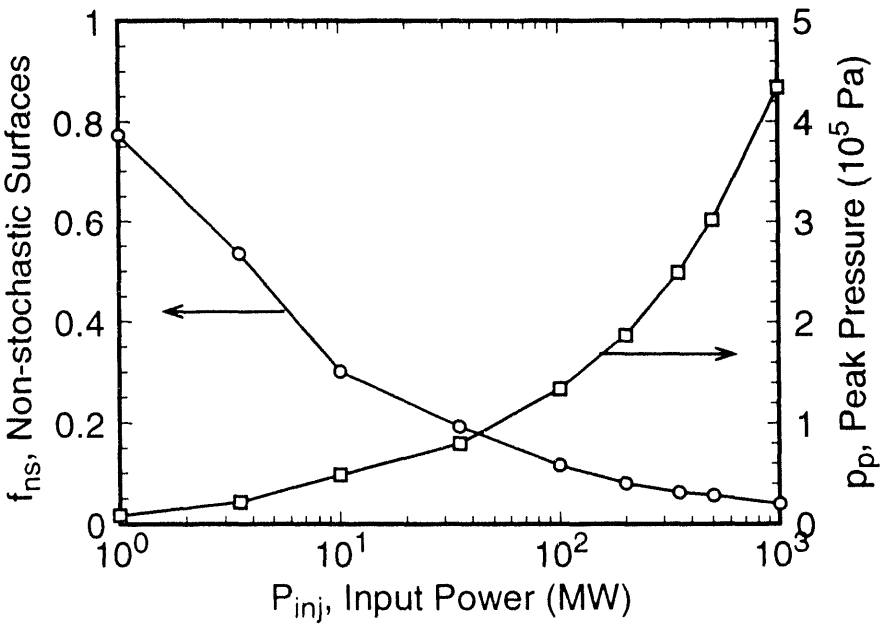

Figure 5: An increase in the injected power leads to an increase in the peak pressure and a steepening of the pressure gradients across each of the islands. The steeper gradients further destabilize the islands and enlarge each island's width. The larger widths manifest themselves as a decrease in the total fraction of non-stochastic surfaces. Both the peak pressure and fraction of non-stochastic surfaces are averaged over 2×10^{-3} τ_r at the end of each simulation.

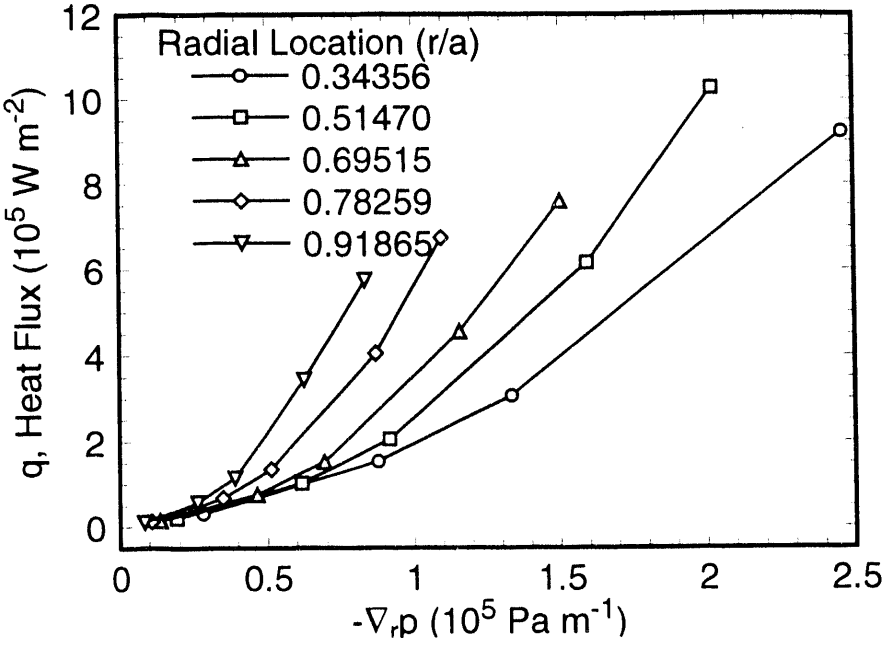

Figure 6: The heat flux is a nonlinear function of the pressure gradient. Each curve is generated based on the heat flux through the center of an island and the mean pressure drop across the center of the two adjacent islands.

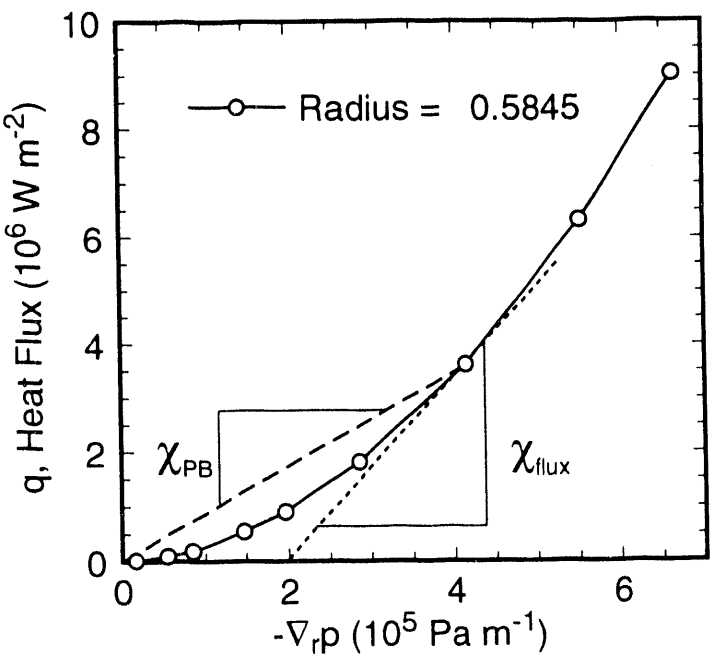

Figure 7: The power balance pressure diffusion coefficient, χ_{PB}, is defined as the ratio of the heat flux to the radial pressure gradient. In contrast, the incremental pressure diffusion coefficient χ_{flux} is defined based on the "local" slope of the curve.

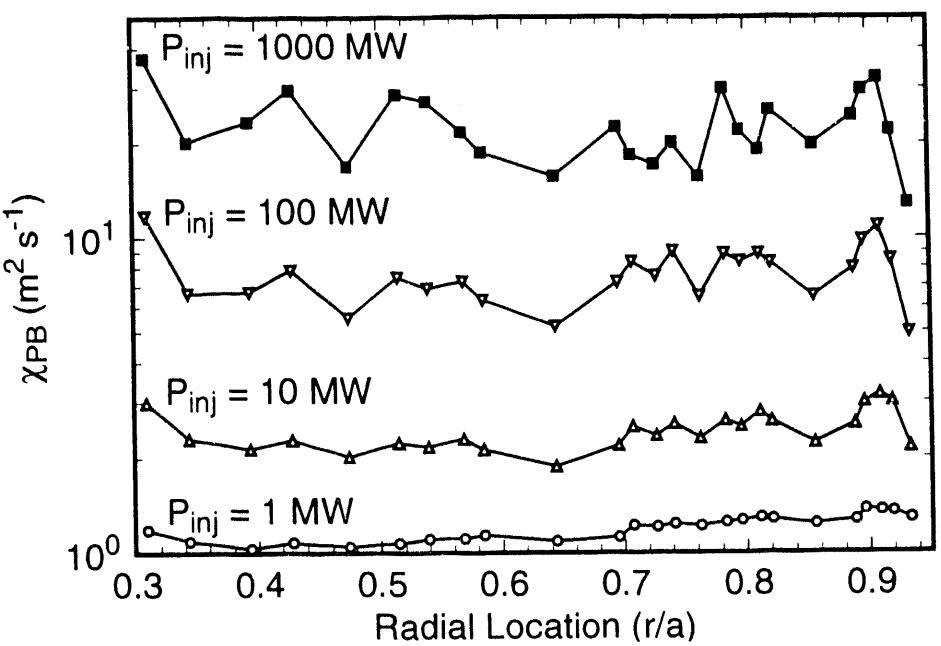

Figure 8: The power balance pressure diffusion coefficient, χ_{PB}, weakly increases from the core to the edge region and sharply increases with the injected power.

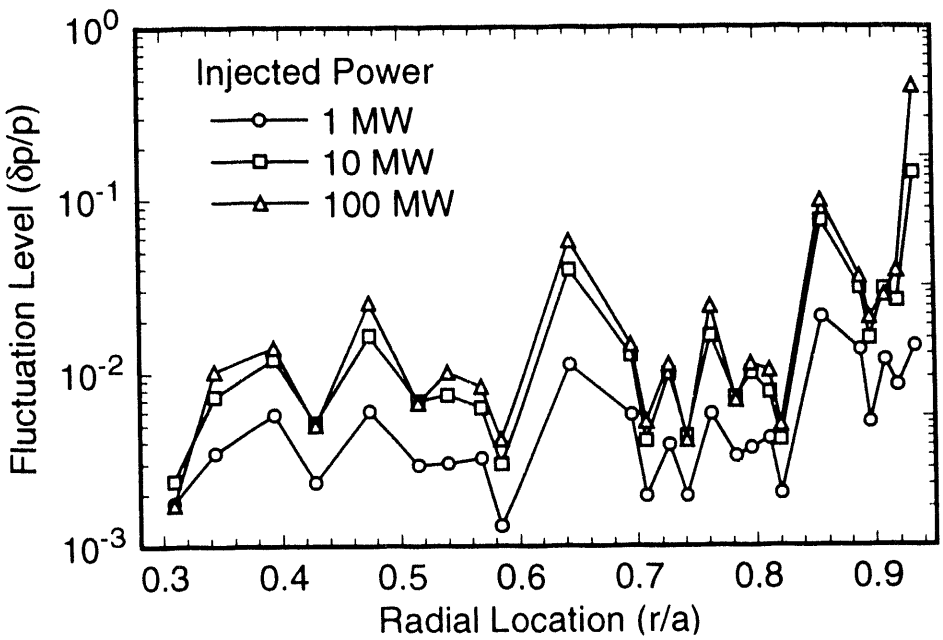

Figure 9: Pressure fluctuation level based on the static rotation of an island structure past a fixed diagnostic. These fluctuation levels increase with injected power, because the island widths increase with injected power. Each fluctuation level is only strictly valid for a single isolated island, rather than the near overlapping island situation in the simulations (see Fig. 1).

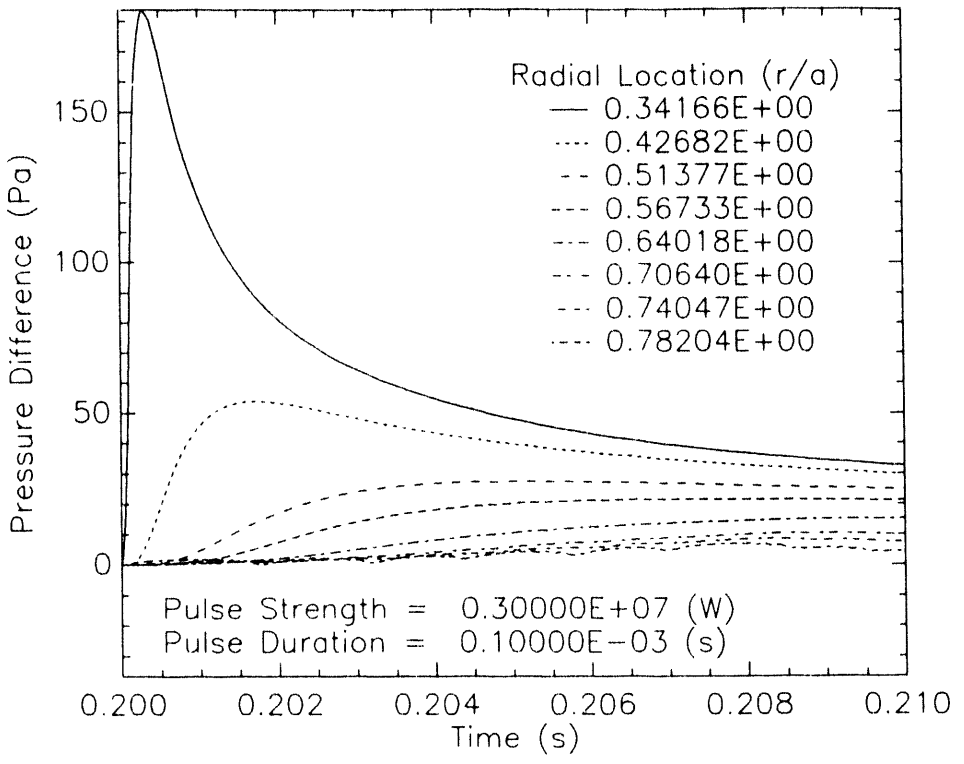

Figure 10: The transient response of the pressure to a heat pulse at a radial location away from the source yields a sharp rise in the pressure followed by a slow decay in the pressure. The pressure difference is computed as the difference between the steady state value of the pressure and the time-varying pressure during the transient. At the outer radii, an accurate determination of the peak of the pulse is corrupted by numerical noise.

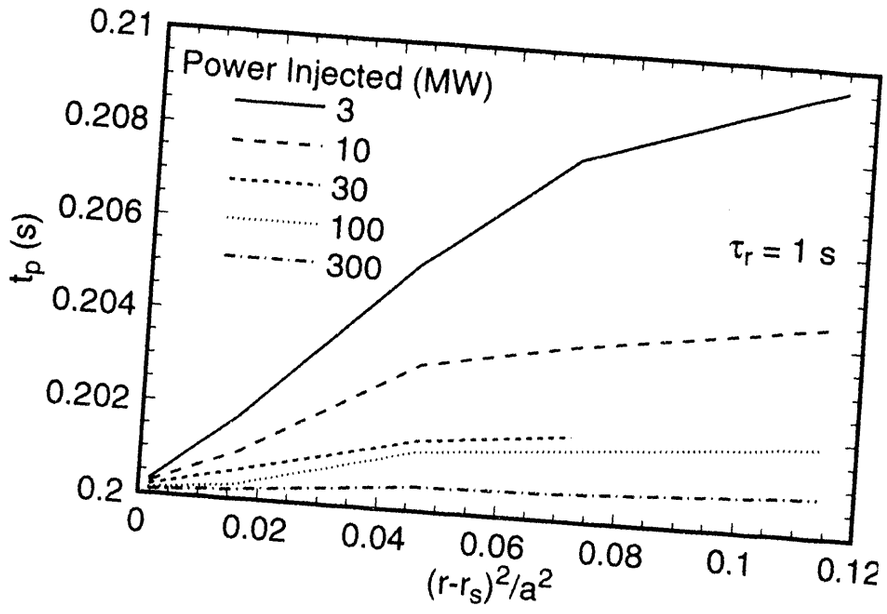

Figure 11: The time-to-peak delay of the heat pulse shortens with an increase in the injected power. The heat pulse is injected at $t_p = 0.2$ s at the source location r_s. The rollover in t_p is caused by the suppression of the pulse due to the fixed pressure at the edge boundary.

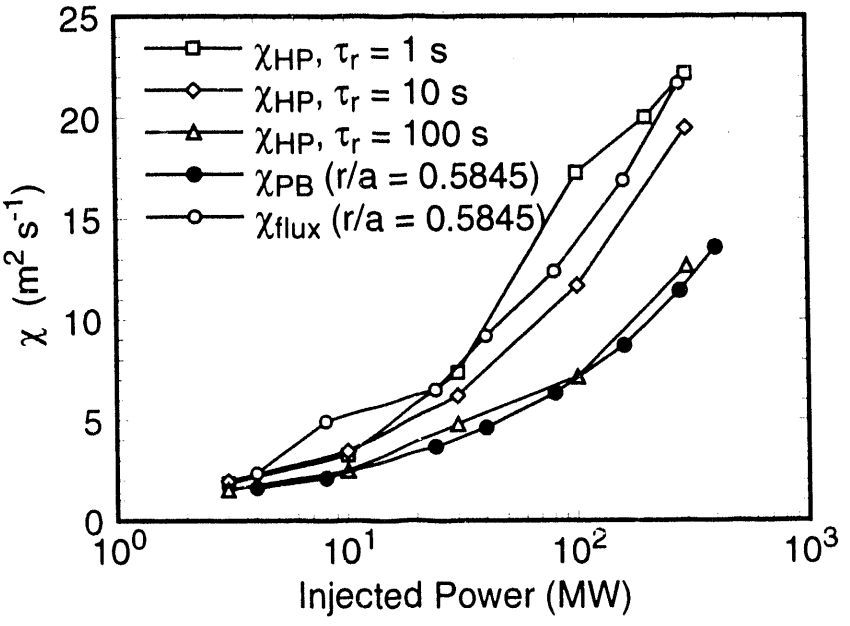

Figure 12: Power balance χ_{PB} and heat pulse χ_{HP} diffusion coefficients increase with the injected power. The power balance diffusion coefficient is based on the radial location of $(r/a) = 0.5845$. Also, χ_{HP} approaches χ_{PB} as τ_r is increased, i.e., as pressure diffusion dominates magnetic diffusion.

DATE
FILMED
4/20/94
END